Ninth International Conference on
THIN-WALLED STRUCTURES – ICTWS2023
Sydney, Australia, Nov 29 – Dec 1, 2023

LOCAL BUCKLING OF WIRE ARC ADDITIVELY MANUFACTURED I-SECTIONS

Ben Weber*, Xin Meng* and Leroy Gardner*

* Imperial College London, London, United Kingdom
e-mails: ben.weber19@imperial.ac.uk, xin.meng15@imperial.ac.uk, leroy.gardner@imperial.ac.uk

Keywords: 3D laser scanning; Digital image correlation; I-section members; Local buckling; Structural testing; Wire arc additive manufacturing (WAAM).

Abstract. *Wire arc additive manufacturing (WAAM), a 3D printing technique for metals, has sparked a great deal of research interest over the past years in the construction sector due to its ability to create sizeable objects of complex shapes, with high deposition rates and relatively low cost. In this study, seven I-section stub columns with different cross-section profiles, printed via WAAM using high strength steel grade ER90S-G welding wire, were tested to investigate their compressive resistance. The WAAM stub column specimens were 3D laser scanned before testing to capture their unique surface undulations and local geometric imperfections inherent to the printing process for correlation with the local buckling test results. The surface displacements and strains of the two flanges and the web were measured during testing using digital image correlation (DIC). The results of the I-section stub column tests generally followed the anticipated trends, with load-carrying capacities above the plastic loads in the stocky range, but reducing normalised capacities in the slender range due to the increased prominence of local buckling.*

1 INTRODUCTION

Wire arc additive manufacturing (WAAM) has shown the potential to significantly impact the construction industry by enabling engineers to create structures that would not be feasible to produce using traditional methods [1]. The ability of this novel manufacturing process to create intricate geometries, such as internal stiffening structures [2] and topologically optimised elements [3], and to strengthen existing structures [4], helps to enhance material efficiency in structural projects. This could ultimately help to reduce the cost and environmental impact of the construction industry as a whole.

Before this vision can be realised, fundamental research into the material and structural behaviour of WAAM needs to be conducted. A number of studies have been carried out to characterise the material behaviour of different grades of carbon steel [5, 6], as well as other 3D printed metallic materials, such as stainless steel [7, 8], aluminium [9] and titanium [9]. Early investigations into the structural performance of WAAM structural elements have been conducted, such as bending tests [10], compression tests [2] and connection tests [11]. However, the local buckling performance of WAAM I-section members has not yet been explored.

In the present study, the local buckling behaviour of seven I-section specimens with varying flange and web slendernesses, manufactured by WAAM using high-strength steel welding wire, has been investigated. The geometric properties of the specimens were analysed with the help of 3D laser-scanning, and the structural behaviour during testing was captured using digital image correlation (DIC). The obtained test results on the WAAM I-section stub columns are compared with the predicted resistances derived from Eurocode 3.

2 DESIGN AND SPECIMEN MANUFACTURE

To investigate the local buckling behaviour of WAAM elements in compression, a total of seven I-section specimens, labelled I1 - I7, were designed with varying web and flange slendernesses, as shown in Figure 1, where c_f is the width of the outstand flange, c_w is the height of the internal web in compression, t_w is the thickness of the web, t_f is the thickness of the flange, and $\varepsilon = \sqrt{235 / f_y}$ is a material parameter defined by the yield stress f_y. Figure 1 also shows the relevant Class 3/4 slenderness limits specified in prEN 1993-1-1 [12]. The cross-sections of the test specimens were dimensioned to cover both Class 1-3 cross-sections and Class 4, as detailed in Table 1, with their nominal height H_{nom}, width B_{nom}, flange thickness $t_{f,nom}$, web thickness $t_{w,nom}$ and length L_{nom} in mm and nominal area A_{nom} in mm^2.

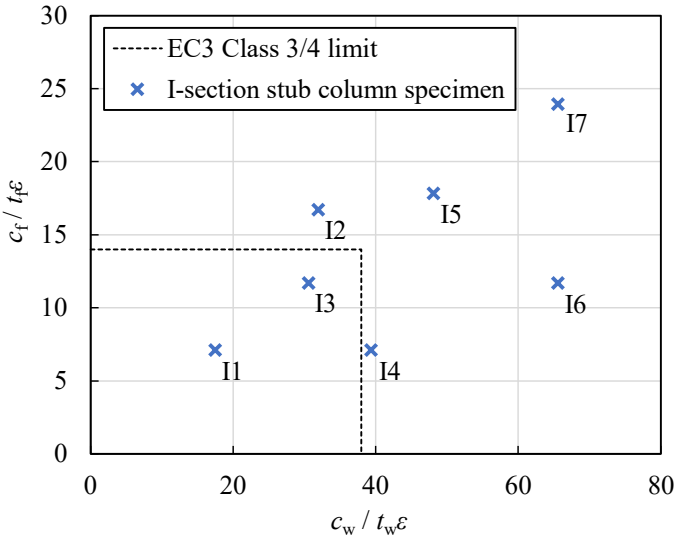

Figure 1: Local web and flange slenderness of the different I-section stub column samples compared to the EC3 Class 3/4 limits.

The I-section stub column specimens, as shown in Figure 2, were manufactured using a 6-axis robotic arm by MX3D, a Dutch company specialised in WAAM 3D printing. The feedstock used for printing was carbon steel grade ER90S-G welding wire with a 1.2 mm diameter. The as-welded mechanical properties of the feedstock wire as well as its chemical composition, provided in the wire certificate are presented in Tables 2 and 3 respectively. As shown in Table 1, two different nominal wall thicknesses - 3.5 mm and 5.0 mm, denoted as ER90-3.5 and ER90-5.0, were employed, and their printing parameters are listed in Table 4.

The manufactured specimens were cut using a bandsaw to their designed length L_{nom}, corresponding to three times their maximum cross-sectional dimension (i.e. H_{nom}). The welding scale present on the surface of the specimens was removed by grit blasting, and the ends of the stub columns were lapped flat to ensure the uniformity of the applied compressive stresses.

Table 1: Design dimensions of the WAAM I-section stub columns.

Specimen ID	H_{nom} (mm)	B_{nom} (mm)	$t_{f,nom}$ (mm)	$t_{w,nom}$ (mm)	L_{nom} (mm)	A_{nom} (mm^2)
I1	50	50	5.0	3.5	150	640.0
I2	80	80	3.5	3.5	240	815.5
I3	80	80	5.0	3.5	240	1045.0
I4	100	50	5.0	3.5	300	815.0
I5	120	120	5.0	3.5	360	1585.0
I6	160	80	5.0	3.5	480	1325.0
I7	160	160	5.0	3.5	480	2125.0

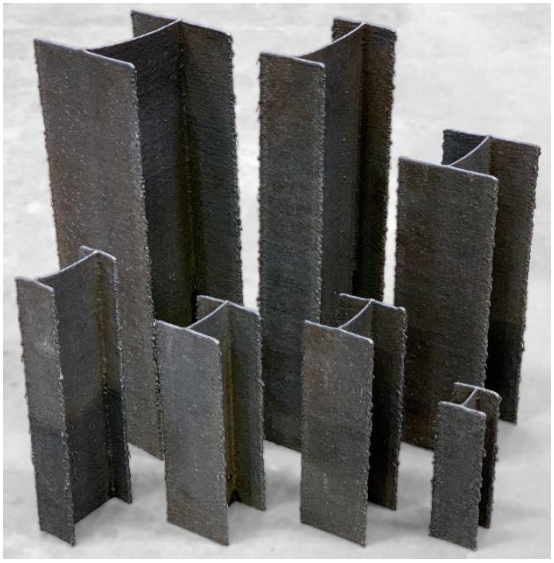

Figure 2: WAAM I-section stub columns.

Table 2: As-welded mechanical properties of ER90S-G wire from wire certificate.

Property	Minimum guaranteed value	Measured value
Yield strength f_y	560 MPa	607 MPa
Ultimate strength f_u	620 MPa	637 MPa
Elongation at fracture ε_f	18 %	18 %
Charpy V-notch impact energy A_v	47 J @ -70 °C	60 J @ -70 °C

Table 3: Chemical composition of ER90S-G wire (in %) from wire certificate.

C	Si	Mn	S	Cu	Cr	Mo	Ni	Co	Fe
0.10	0.71	1.89	0.011	0.025	0.04	0.44	0.05	0.013	Balance

Table 4: Process parameters associated with the different wall thicknesses of the I-sections.

	ER90-3.5	ER90-5.0
Nominal current (A)	102	117
Nominal voltage (V)	14.6	15.6
Torch speed (mm/s)	12	9
Stick out (mm)	9-12	9-12
Interpass temperature (°C)	350	350
Shield gas composition	98 % Ar, 2 % CO_2	98 % Ar, 2 % CO_2
Shield gas flow rate (l/min)	16.0	16.0
Wire feed rate (m/min)	2.3	2.7
Average layer height (mm)	1.09	1.22
Nominal layer width (mm)	3.5	5.0

3 GEOMETRIC ANALYSIS

3.1 Data acquisition and processing

The surface undulations inherent to the additive manufacturing process can affect the structural behaviour of WAAM elements [2]. To accurately capture these undulations and analyse the geometric properties of the I-section stub columns, the specimens were 3D laser scanned using a FARO ScanArm prior to testing. This process enabled the acquisition of a point cloud of the full geometry of the I-sections with an accuracy of 0.1 mm. The point cloud was post-processed into a surface mesh using Geomagic Wrap [13], and then contour plots with a spacing of 0.1 mm were extracted longitudinally from the mesh object using the software package Rhino [14] to facilitate the analysis of key geometric properties, as shown in Figure 3;

the adopted spacing of the contour plots was shown to accurately capture the surface undulations without creating excessive data [5].

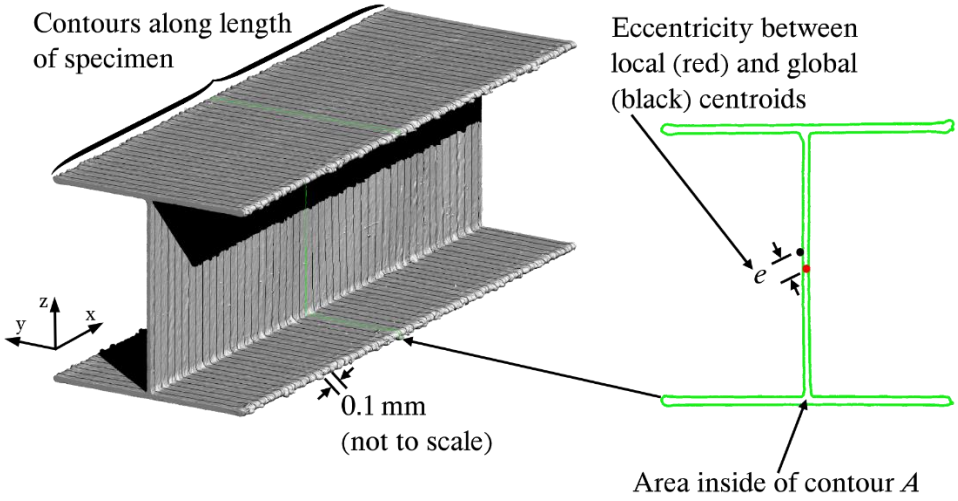

Figure 3: Post-processing of the laser-scanned data of WAAM I-section stub columns.

3.2 Geometric properties

The geometric properties determined using the described laser-scanning process are presented in Table 5, including the average cross-section height H, width B, flange thickness t_f, web thickness t_w, length L and eccentricity e as well as the average cross-sectional area A. The measured cross-section height H was shown to be slightly lower than the nominal value for all specimens with an average ratio between the measured and nominal values equal to 0.99, while the cross-section width B was shown to be higher than the nominal value with an average measured-to-nominal ratio of 1.05. The thicknesses of the elements, however, deviated further from their nominal values - the average ratio of the measured-to-nominal thickness was equal to 0.88 and 0.93 for those with t_{nom} of 5.0 mm and 3.5 mm respectively.

Table 5: Measured geometric properties of the WAAM I-section stub columns.

Specimen ID	H (mm)	B (mm)	t_f (mm)	t_w (mm)	L (mm)	e (mm)	A (mm^2)	H/H_{nom}	B/B_{nom}	$t_f/t_{f,nom}$	$t_w/t_{w,nom}$	A/A_{nom}
I1	49.2	54.0	4.42	3.23	149.7	0.554	633.4	0.984	1.080	0.883	0.924	0.990
I2	79.2	83.6	3.20	3.22	240.7	0.614	806.5	0.990	1.045	0.915	0.921	0.989
I3	79.1	83.6	4.36	3.30	240.3	0.470	991.5	0.989	1.045	0.872	0.942	0.949
I4	98.9	53.4	4.45	3.32	300.4	0.612	807.8	0.989	1.068	0.890	0.949	0.991
I5	118.8	123.1	4.40	3.28	360.3	0.771	1477.9	0.990	1.026	0.879	0.938	0.932
I6	158.5	83.5	4.45	3.25	479.8	0.906	1263.1	0.991	1.044	0.889	0.928	0.953
I7	158.7	163.0	4.45	3.30	480.3	0.747	1979.7	0.992	1.019	0.891	0.943	0.932

4 LOCAL BUCKLING TESTS ON WAAM I-SECTION STUB COLUMNS

4.1 Test setup

Testing of the WAAM I-section stub column specimens was carried out using a 3500 kN Instron hydraulic testing machine, as shown in Figure 4. The top end plate was equipped with a ball seating, which ensured that any out-of-squareness of the specimen ends were compensated. Hardened steel end plates were employed on both the top and bottom of the samples to spread the load uniformly and prevent damage to the testing equipment. Three stereo

digital image correlation (DIC) systems, with a total of six individual cameras, were employed to capture the surface displacements of both flanges and the web of the I-section stub columns during testing. A schematic test setup showing the top down view of the camera layout is presented in Figure 5. A speckle pattern, consisting of random white dots on a black background, was applied via spray painting to the surface of the samples to provide trackable features for DIC. Additional LED lights were placed around the sample during testing to ensure a good image quality for the DIC system.

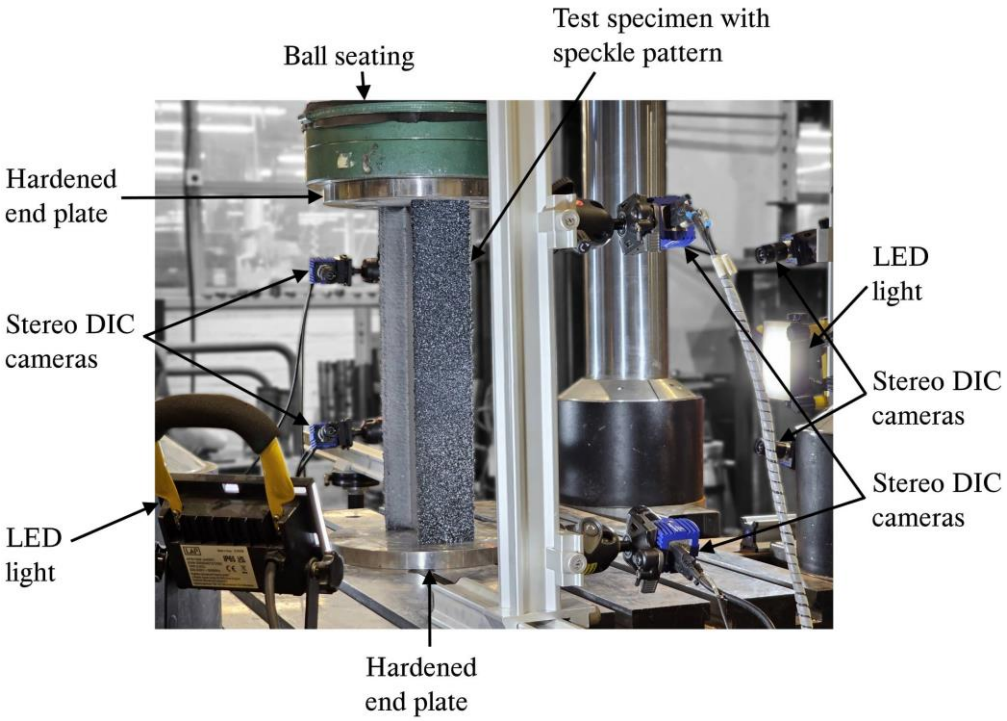

Figure 4: Test setup for WAAM I-section stub columns.

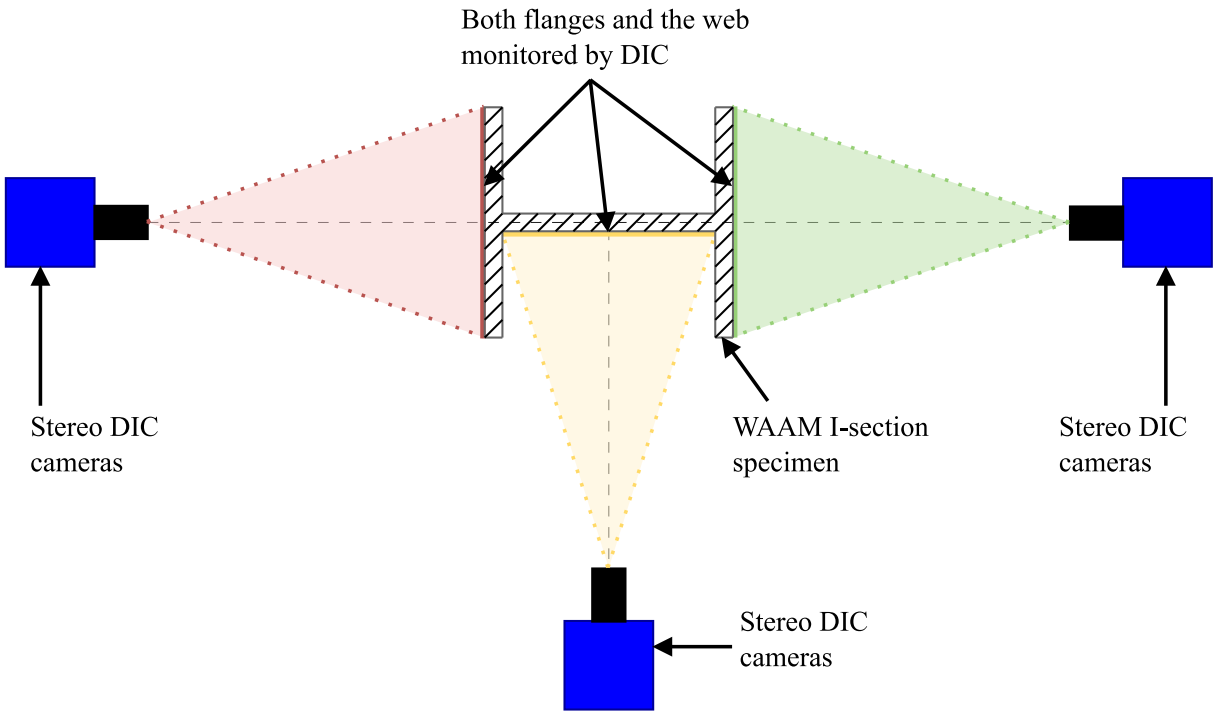

Figure 5: Top down schematic view of the DIC setup.

Testing of the samples was carried out under displacement control, with a rate corresponding to a strain rate of 0.1%/min. DIC images were captured at a rate of 0.5 Hz using the software package DaVis [15], with the measurements of the load cell, integrated into the testing machine, directly captured by the DIC system and synchronised to the image capture rate.

4.2 Test results and discussion

The failure modes of the I-section stub column samples, are presented in Figure 6 and the key test results are presented in Table 6, including the ultimate capacity of the sections N_u as well as the end-shortening at ultimate load δ_u. The ultimate capacity is also normalised by the cross-sectional plastic load N_{pl} equal to the measured average cross-sectional area A multiplied by the material yield strength obtained from as-built coupon tests f_y. Lastly, the web ($c_w/t_w\varepsilon$) and flange ($c_f/t_f\varepsilon$) slendernesses, derived based on the laser-scan data, are also presented in Table 6. The axial load-end shortening curves of the I-section stub column tests are shown in Figure 7, with δ being the end shortening and N being the axial load. Normalised load-end shortening curves are also presented in Figure 8, where the load is normalised by the cross-sectional plastic load N_{pl} and the end shortening is normalised by the theoretical end shortening at first yield $\delta_y = f_yL/E$ with the Young's modulus E obtained from as-built coupon tests. The normalised ultimate capacities of the tested WAAM stub columns are plotted along with their web and flange slendernesses in Figures 9 and 10 respectively, and compared against the slenderness limits given in prEN 1993-1-1 [12] for plated elements in pure compression. The specimens are highlighted as either web or flange governing depending on the ratio of the element slenderness $c/t\varepsilon$ to the respective EC3 Class 3/4 slenderness limit. The element with the higher ratio is deemed to be governing.

Figure 6: I-section stub columns after testing.

Table 6: Test results for the WAAM I-section stub column tests.

Specimen ID	N_u (kN)	δ_u (mm)	$c_f/t_f\varepsilon$	$c_w/t_w\varepsilon$	N_u/N_{pl}
I1	397.2	3.53	8.0	17.4	1.380
I2	428.9	1.12	17.5	31.4	1.170
I3	555.2	1.59	12.8	29.7	1.232
I4	418.5	1.56	7.8	37.7	1.140
I5	703.3	1.35	18.9	46.6	1.047
I6	548.6	2.27	12.5	64.0	0.956
I7	799.0	1.47	25.0	63.1	0.888

All tested WAAM stub columns exhibited the classic local buckling mode for I-section profiles. Specimens I2 and I5, despite being classified as Class 4, were shown to be able to reach their respective plastic load N_{pl}. Overall, the EC3 Class 3/4 slenderness limits were shown to be safe-sided. Further investigations are needed to improve the accuracy and assess the reliability of the EC3 cross-section design rules for WAAM elements.

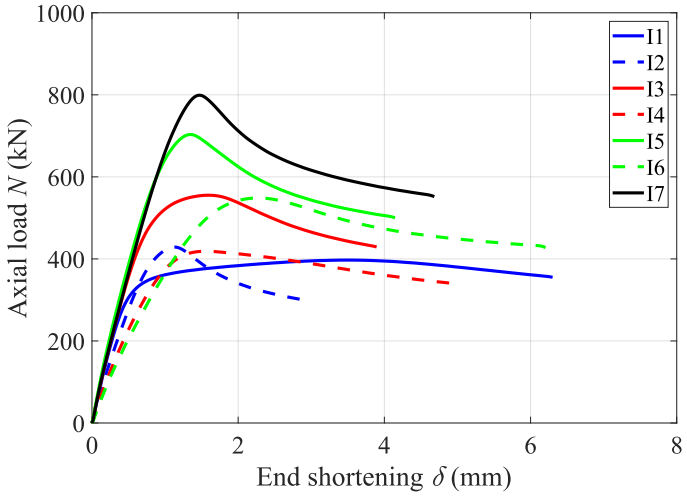

Figure 7: Axial load-end shortening curves from the WAAM I-section stub column tests.

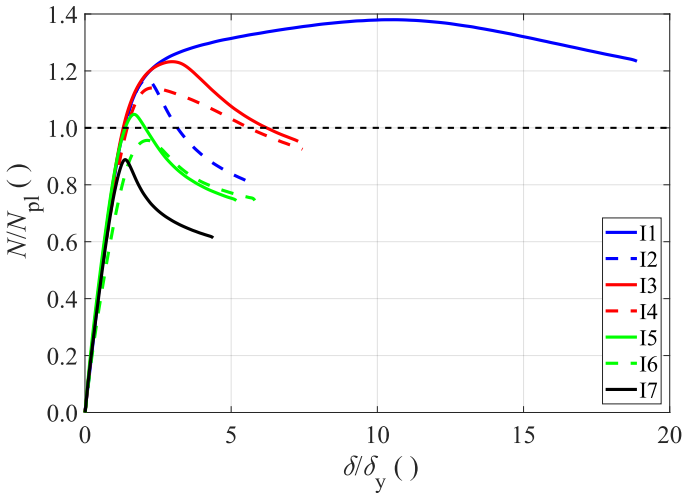

Figure 8: Normalised load-end shortening curves from the WAAM I-section stub column tests.

5 CONCLUSIONS

In the present study, seven I-section stub column specimens, manufactured via wire arc additive manufacturing (WAAM) using ER90S-G welding wire as the feedstock material, have been tested. The studied cross-sectional profiles were designed to cover a wide range of flange and web slendernesses. 3D laser-scanning was employed to accurately capture the intricate geometry of the additively manufactured specimens and to compare it against the geometry of the nominal design. The stub column specimens were tested using fixed ended boundary conditions and the test data was captured using non-contact digital image correlation (DIC). The local buckling behaviour of the samples was found to be similar to traditionally manufactured sections. Existing Class 3/4 slenderness limits specified in prEN 1993-1-1 were shown to be safe-sided.

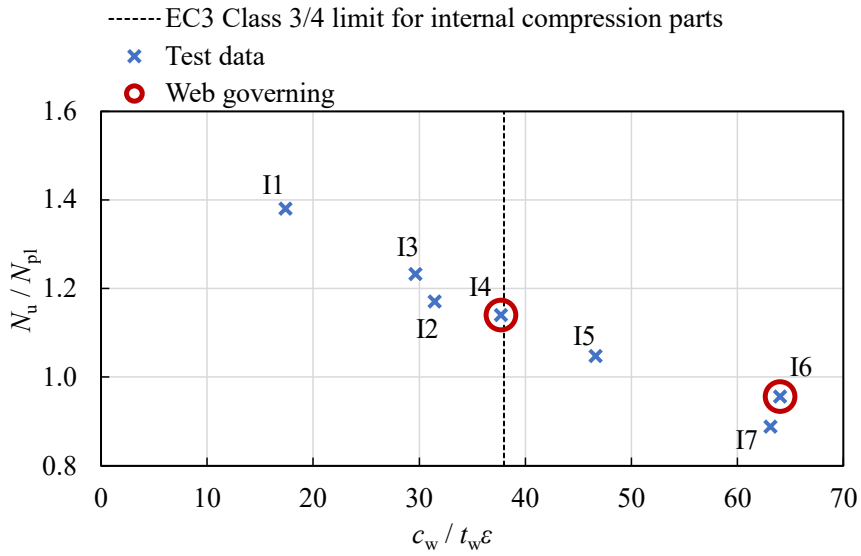

Figure 9: Comparison of obtained test data on WAAM I-section stub columns with EC3 slenderness limits for internal compression parts.

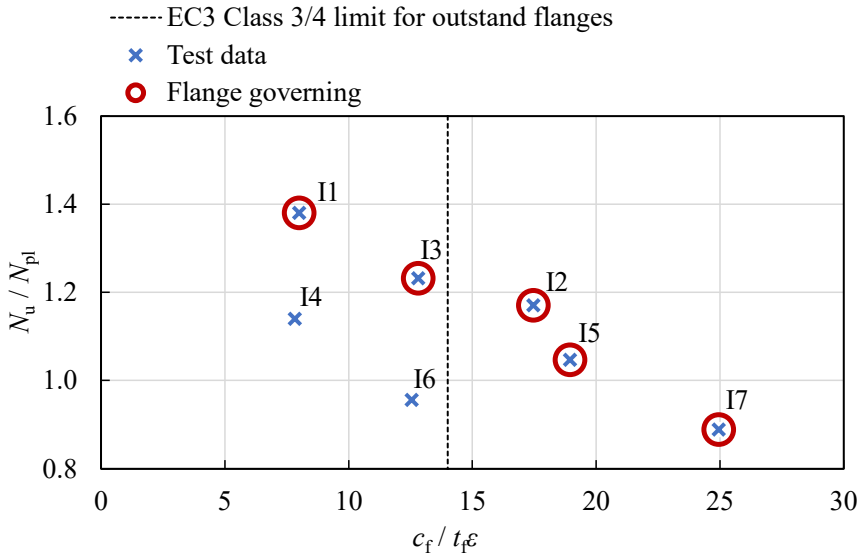

Figure 10: Comparison of obtained test data on WAAM I-section stub columns with EC3 slenderness limits for outstand flanges.

ACKNOWLEDGMENTS

This study was possible thanks to funding and support from the Shimizu Corporation and from the National Research Fund of Luxembourg.

REFERENCES

[1] Gardner L., "Metal additive manufacturing in structural engineering–review, advances, opportunities and outlook", *Structures*, **47**, 2178 - 2193, 2023.

[2] Meng X., Weber B., Nitawaki M. and Gardner L., "Optimisation and testing of wire arc additively manufactured steel stub columns", *Thin-Walled Structures*, **189**, 110857, 2023.

[3] Ye J., Kyvelou P., Gilardi F., Lu H., Gilbert M. and Gardner L., "An end-to-end framework for the additive manufacture of optimized tubular structures", *IEEE Access*, **9**, 165476 - 165489, 2021.

[4] Kloft H., Schmitz L.P., Müller C., Laghi V., Babovic N. and Baghdadi A., "Experimental application of robotic wire-and-arc additive manufacturing technique for strengthening the I-beam profiles", *Buildings*, **13**(2), 366, 2023.

[5] Huang C., Kyvelou P., Zhang R., Britton T.B. and Gardner L., "Mechanical testing and microstructural analysis of wire arc additively manufactured steels", *Materials & Design*, **216**, 110544, 2022.

[6] Weber B., Meng X., Zhang R., Nitawaki M., Sagawa T. and Gardner L., "Tensile behaviour of WAAM high strength steel material and members", *Materials & Design* (submitted), 2023.

[7] Hadjipantelis N., Weber B., Buchanan C. and Gardner L., "Description of anisotropic material response of wire and arc additively manufactured thin-walled stainless steel elements", *Thin-Walled Structures*, **171**, 108634, 2022.

[8] Laghi V., Palermo M., Tonelli L., Gasparini G., Ceschini L. and Trombetti T., "Tensile properties and microstructural features of 304L austenitic stainless steel produced by wire-and-arc additive manufacturing", *The International Journal of Advanced Manufacturing Technology*, **106**(9), 3693 - 3705, 2020.

[9] Derekar K., "A review of wire arc additive manufacturing and advances in wire arc additive manufacturing of aluminium", *Materials science and technology*, **34**(8), 895 - 916, 2018.

[10] Huang C., Meng X. and Gardner L., "Cross-sectional behaviour of wire arc additively manufactured tubular beams", *Engineering Structures*, **272**, 114922, 2022.

[11] Guo X., Kyvelou P., Ye J., Teh L.H. and Gardner L., "Experimental investigation of wire arc additively manufactured steel single-lap shear bolted connections", *Thin-Walled Structures*, **181**, 110029, 2022.

[12] prEN 1993-1-1:2020, Eurocode 3 - Design of steel structures - Part 1-1: General rules and rules for buildings, European committee for standardization, 2020.

[13] Oqton, Inc, Geomagic Wrap 2017, https ://www.oqton.com/geomagic-wrap, Version 2017.0.2:64.

[14] Robert McNeel & Associates, Rhino 6, https://www.rhino3d.com/, Version 6 SR35.

[15] LaVision GmbH, DaVis 10, https://www.lavision.de/en/products/davissoftware/, Version 10.2.1.